RPE | Radiation Physics & Engineering
A Peer-Reviewed Journal
Published by K.N. Toosi University of Technology
http://rpe.kntu.ac.ir
Research Article

Radiation Physics and Engineering 2026; ?(?):?–?

Toward a Monte Carlo-driven 3D dose verification framework for IMRT: A pilot implementation for nasopharyngeal carcinoma

Elie Hoseinian-Azghadi[a], Laleh Rafat-Motavalli[a,*], Hashem Miri-Hakimabad[a,b], Vida Khodabandeh-Baygi[a,b], Taylan Tuğrul[c], Mahdieh Dayyani[b,d]

[a] *Physics Department, Faculty of Science, Ferdowsi University of Mashhad, Mashhad, Iran*
[b] *Research and Education Department, Reza Radiotherapy and Oncology Center, Mashhad, Iran*
[c] *Department of Radiation Oncology, Medicine Faculty of Van Yüzüncü Yl University, Van, Turkey*
[d] *Radiation Oncology Department, Reza Radiotherapy and Oncology Center, Mashhad, Iran*

HIGHLIGHTS

- A full Monte Carlo simulation of the Siemens Artiste linac and 160-leaf MLC was implemented using MCNPX 2.6.0.
- The framework achieved a 3D gamma passing rate of 97.1% (3%/3 mm) for a nasopharyngeal carcinoma plan.
- The model establishes the foundation for a localized, patientspecific Monte Carlo verification tool.

ABSTRACT

Monte Carlo (MC) methods are considered a complementary method for dose verification in radiation therapy. This study aims to simulate the Artiste head and the Siemens 160 Multileaf Collimator (MLC) using MCNPX 2.6.0 to enhance dose verification accuracy in Intensity-Modulated Radiation Therapy (IMRT) treatment plans. The MC-based calculations were benchmarked against commissioning-measured data and an MLC test field. A comparison between MC-based and treatment planning system (TPS)-based dose maps was made for beams of a typical complicated IMRT plan. The results demonstrated a 3D gamma passing rate (GPR) of 97.1% with 3%/3mm criteria and a 10% dose threshold, indicating the accuracy of the MC model. Based on the acceptable GPRs, the provided model has sufficient accuracy. It has been confirmed that the MC calculations can be carried out within a reasonable computation time, taking approximately 10 minutes per beam and less than 2 hours for a typical 9-beam IMRT plan. This is possible with a specific, powerful CPU configuration used for MC verification of such a complicated IMRT plan.

KEYWORDS

Monte Carlo code
Intensity-Modulated Radiation Therapy (IMRT)
Patient-specific QA
Dose verification

HISTORY

Received:
Revised:
Accepted:
Published:

1 Introduction

Intensity-Modulated Radiation Therapy (IMRT) aims to deliver the prescribed dose to a defined target volume with high accuracy, thereby improving outcomes (Zhu et al., 2021). To deliver standard doses and achieve automatic, precise beam shaping, treatment planning systems (TPSs) design IMRT dose distributions with steep dose gradients using appropriate Multileaf collimator (MLC) configurations (Zhang et al., 2015). The consequent complexity of IMRT plans, together with the lack of accurate MLC modeling in TPSs, necessitates independent dose verification through the pretreatment quality assurance (QA) process known as patient-specific QA (PSQA) (Miften et al., 2018). Experimental methods commonly used for PSQA are time-consuming and, if they detect an unacceptable plan, cannot identify the source of the error or its impact on the patient dose distribution (Nelms et al., 2013; Kry et al., 2014). Therefore, calculation-based dose verification is recommended as part of PSQA (Stapleton et al., 2005). The Monte Carlo (MC) method is considered the most accurate computational tool for such validations. It is regarded as the gold standard for radiation transport calculations, especially for small radiation beams, irregular surfaces, and heterogeneous media (Chetty et al., 2007; Palmans et al., 2018; Girardi et al., 2019). Several researchers have modeled various Linac machines using MC simulation. For these simulations, general-purpose MC software such as EGSnrc, GEANT4, PENELOPE, and

*Corresponding author: rafat@um.ac.ir

https://doi.org/

MCNP has been widely used by MC investigators (Paschal et al., 2022; Kandlakunta et al., 2019; Sempau et al., 2011; Lewis et al., 1999; Park et al., 2021).

Nevertheless, to the best of our knowledge, no comprehensive Monte Carlo study has incorporated both the Artiste linear accelerator head and detailed MLC modeling for IMRT plans. Sadrollahi et al. (Sadrollahi et al., 2019) and Turul et al. (Tuğrul and Eroğul, 2019) previously simulated the Artiste linac head using GEANT4 and EGSnrc, but neither considered the MLC geometry. Consequently, certain conditions may arise in which neither the TPS nor existing MC-based tools can detect potential errors in the treatment plan (Nelms et al., 2013; Kry et al., 2019; Kerns et al., 2017). Furthermore, the high cost of commercially available MC-based IMRT QA tools may also encourage radiotherapy clinics to develop an in-house MC-based code for dose verification. Therefore, our clinic has decided to enhance our current measurement-based PSQA process by incorporating an MC-based dose verification tool for IMRT plans using the Artiste Linac with 160 MLC (manufactured by Siemens Medical Solutions Inc., Germany).

While MC-based dose calculation and verification have been widely reported for various linear accelerator models, particularly Elekta HD and Varian TrueBeam, the present work constitutes a distinct and novel contribution specific to Siemens linear accelerators, focusing on the Siemens Artiste system.

This work presents the first demonstration of the technical feasibility and dosimetric accuracy of evaluating a Siemens Artiste IMRT plan using MCNPX. This study introduces two innovations: a complete Monte Carlo model of the Siemens 160-MLC in MCNPX, the first of its kind for a Siemens MLC in this code. Second, this study conducts a full Monte Carlo (MC) simulation of a real clinical IMRT plan, capturing the complexity of delivery, including multiple gantry angles, numerous segments per beam, segment-specific monitor units, and a patient-specific voxelized anatomical model.

This work addresses a critical gap in the literature. Although comprehensive MCbased dose calculation and verification frameworks have been developed for other linear accelerator vendors, particularly Varian and Elekta, these workflows are inherently machine-specific. They cannot be directly transferred to Siemens linear accelerators without extensive remodeling of the accelerator head and beamshaping components.

Moreover, the number of Monte Carlo studies that have considered Siemens systems has generally been restricted in scope, often focusing on jaw-defined fields, water phantom simulations, rather than full patient-specific IMRT plan simulations. These limitations have therefore precluded a realistic end-to-end Monte Carlo evaluation of Siemens-based clinical IMRT treatments. Consequently, the lack of a comprehensive, patient-specific Monte Carlo framework for Siemens linear accelerators necessitated the present study.

The primary goal was to develop an MC-based independent dose verification tool to overcome limitations of existing treatment planning systems and improve patient-specific quality assurance. A detailed MCNPX model of the Artiste Linac head and Siemens 160-MLC was thoroughly benchmarked against commissioning measurements and MLC tests. After validation, a dosimetric comparison between MC-calculated and TPS-based dose maps was performed for a complex clinical IMRT plan.

2 Materials and Methods

The MCNPX code (version 2.6.0) was employed to simulate a 6 MV flattened photon beam from a Siemens Artiste linear accelerator, using geometrical data provided by the vendor (Siemens Healthcare, Erlangen, Germany) (Hendricks et al., 2008). The MC simulations were performed in three steps using the surface source write/read (SSW/SSR) feature to generate phase space files (PSF), which captured the positions, directions, and energies of particles (photons, electrons, and positrons) at specific surfaces. In the first stage, the primary electron source and upstream fixed head components were modeled to produce a primary PSF at 19 cm from the target. This PSF served as a surface source in the second stage, generating a secondary PSF at 46.9 cm downstream of the target, accounting for beam modifiers such as jaws and 160 MLCs. In the third stage, after adjusting the collimator and gantry, the secondary PSF was used to irradiate the phantom/patient, enabling dose distribution estimation in the regions of interest. For all simulations, the electron (ECUT) and photon (PCUT) cut-off energies were set to 0.5 MeV and 0.01 MeV, respectively.

Dose distributions were scored using rectangular energy-deposition mesh tallies per history (in MeV.cm^{-3}), with a 1 mm grid size for non-patient simulations; however, in patient model calculations, the grid size matched the voxel dimensions. For MLC and IMRT plan tests, mesh tally outputs were converted into dose per monitor unit (cGy/MU) using a coefficient derived from machine-specific reference conditions (i.e., the same situation as the machine is calibrated; field size of 10×10 cm^2, depth of maximum dose, 100 cm SSD, etc). (Das et al., 2008), and the total dose distribution was obtained by applying appropriate monitor units (MUs) for all segments.

2.1 Generating the primary PSF

The fixed components of the linear accelerator head - comprising the X-ray target, primary collimator, exit window, flattening filter, ionization chamber, and mirror - were modeled based on vendor-provided data regarding material composition, densities, and geometrical features. To improve agreement between simulated and measured dose distributions, the primary electron beam energy and spatial distribution parameters were fine-tuned. Primary electron energy was sampled from Gaussian spectra with mean energies ranging from 6.3 to 6.9 MeV (in 0.1 MeV increments) and a standard deviation of 0.297 MeV. Each energy produced a primary phase space file (PSF), and the secondary PSFs were used to calculate percentage depth-dose (PDD) curves in a water phantom, with jaws and MLC settings corresponding to a standard 10×10 cm^2

Table 1: Source-specific model parameters for 6 MV flattened beams.

Parameter	Simulation Set 1	Simulation Set 2
Primary electron energy spectrum	Gaussian	Gaussian
Mean electron energy (MeV)	6.58	6.58
Variable values of Mean electron energy (MeV)	6.3, 6.4, 6.5, 6.7, 6.8, 6.9	
Standard deviation of electron energy (MeV)	0.297	0.297
Primary electron beam shape	Cylindrical	Cylindrical
Source distribution	Uniform	Gaussian
Starting point for source width/FWHM in x- and y-direction	2.0 mm	1.0 mm
Variable values of source width/FWHM	2.5, 3.0, 3.5, 4.0 mm	1.25, 1.50, 1.75, 2.00 mm
Source position in the MCNPX coordinate system	(0, 0, 0)	(0, 0, 0)
Direction of beam central axis	Z direction	Z direction
Position of surface for developing primary phase-space file	Z = 19 cm	Z = 19 cm
Position of surface for developing secondary phase-space file	Z = 46.8 cm	Z = 46.8 cm

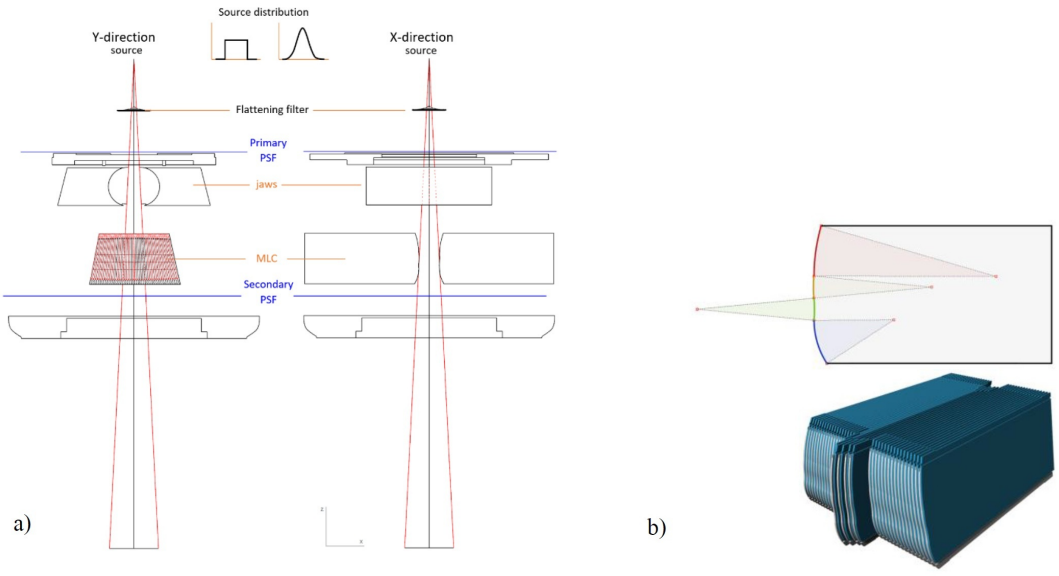

Figure 1: a) The schematic view of simulated Siemens Artiste linear accelerator head, b) The curved shape of the leaf end and the simulated 160 MLCTM bank.

field size. In addition, the primary electron beam's spatial distribution was adjusted to match lateral dose profile (LDP) measurements across square fields ranging from 2×2 cm^2 to 20×20 cm^2, particularly in the penumbra region. The electrons were either uniformly or Gaussian distributed in the x- and y-directions. To adjust the primary electron beam size, a series of PSFs was generated for uniformly distributed sources with diameters between 2.0 and 4.0 mm, and for Gaussian distributed sources with full-width at half-maximum (FWHM) values between 1.0 and 2.0 mm. For further validation, the output factor- defined as the ratio of the absorbed dose for a given field size to that of a reference field- was measured at a 10 cm depth in a water phantom and normalized to a 10×10 cm^2 field size. The measurements were performed using an IBA CC04 ionization chamber (IBA Dosimetry, Bartlett, TN) with a 4 mm diameter and 3.6 mm length in the water phantom, with a source-to-surface distance (SSD) of 100 cm. The schematic view of the simulated linear accelerator head and the positions of the PSF surfaces are presented in Fig. 1-a.

Table 1 shows the starting values of corresponding source-specific parameters that generate the primary PSFs.

2.2 MLC test

The Siemens single-focused 160 MLC consists of two banks, each containing 80 leaves. The leaves are categorized into four types (I, II, III, IV), with minor geometrical variations between the upper and lower leaf designs. All leaves have a width of 5 mm at the isocenter and feature rounded ends shaped by four curved sections. A detailed Monte Carlo simulation of the 160 MLC has been performed using MCNPX. Leaf positions and rotation angles, accounting for the pie-shaped design and tilting, were calculated using in-house software that generated the corresponding cell and surface cards for MCNPX input. Rhinoceros 3D® software was also employed to simulate the entire MLC leaf package (Fig. 1-b), particularly for small fields and complex IMRT plans to verify the accuracy of the MLC geometry. To validate the MLC model, a FOURL MLC test from the Elekta Express QA package was modeled in MC calculations (IMPAC, 2020). The FOURL field is a step-and-shoot field with four abutted L-shaped segments with the gantry and the collima-

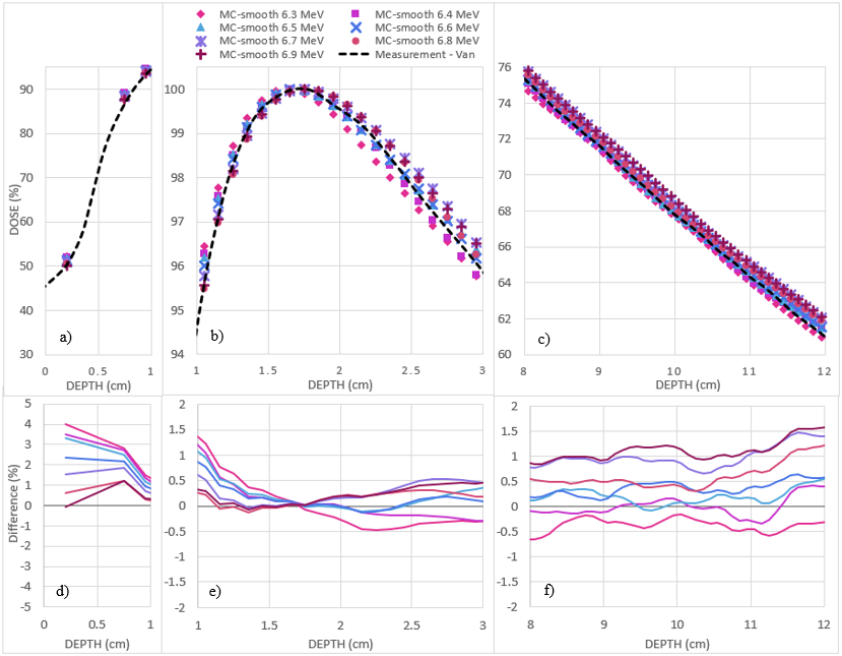

Figure 2: a, b, and c) Depth doses for 6 MV flattened beams with 10 cm × 10 cm filed size and varying mean energy of primary electron beam, and, d, e, and f) dose differences with respect to measured PDDs.

tor rotation angle at 0°. The test was performed in a 15 cm slab phantom and with a source-to-surface distance (SSD) of 90 cm to detect the semi-tongue-and-groove effect at the leaf-side junctions using film dosimetry (Hernandez et al., 2022). The Radiochromic film used in this study was Gafchromic EBT3 (Gafchromic, International Specialty Products, Wayne, NJ), with sheet dimensions of 20.3 cm × 25.4 cm. The films were calibrated using a Farmer® Ionization Chamber 30013 and scanned with a Microtek ScanMaker 9800XL scanner at 100 dpi in RGB mode with 48 bits per channel. An in-house MATLAB code and a triple-channel dosimetry protocol were used to calibrate EBT3 films. Dose profiles along the leaf junctions were extracted at an off-axis position of 2 cm and averaged over a 1 cm region. These profiles were then compared with MC simulations and TPS calculations, both of which were sampled using a dose grid resolution of 1 mm.

2.3 IMRT treatment plan simulation

A complex IMRT treatment plan for nasopharyngeal carcinoma (NPC) has been simulated using the MCNPX 2.6.0 Monte Carlo code to assess the validation of our model. The NPC treatment plan consisted of a nine-field static gantry configuration and 10-25 beam segments, developed using the RayStation® Treatment Planning System (RaySearch Laboratories, Stockholm, Sweden). For each segment, beam coordinates (describing the position and orientation of the linac head), the corresponding number of MUs, the collimator rotations, and the positions of jaws and each leaf in the MLC were extracted from the RayStation treatment plan files. To generate a computational voxel-based phantom for use in the MC simulations, the DICOM files from the CT simulation were converted using in-house MATLAB code. The generated phantom was produced in the two outermost boxes of voxels with dimensions of $167 \times 80 \times 232$ and $485 \times 59 \times 241$, with voxel size of $0.9766 \times 3.0 \times 0.9766$ mm^3 for head and neck parts, respectively. Seven materials (air, lung, adipose, soft tissue, trabecular bone, cortical bone, and teeth) were provided, and ICRP Publication 89 reference data were used to describe the phantoms' material composition (Valentin, 2002).

2.4 Statistical analysis

To compare MC-based data with experimental/TPS-based reference datasets, two metrics, dose difference (DD) and gamma index, were used. Dose difference values were evaluated for Percentage Depth Dose (PDD), Lateral Dose Profile (LDP), and output factor comparisons. For the MLC test, DD values were used to compare dose profiles. In the IMRT plan, gamma passing rates (GPRs) were reported with criteria of 3%/3 mm and 3%/2 mm.

3 Results

3.1 Initial modeling-PDDs, profiles, and output factors

In our Monte Carlo simulations, a total of 2.7×10^{10} particle histories were processed, yielding statistical uncertainties in the absorbed dose measurements of less than 0.1%. The MC simulations were performed until the relative statistical uncertainties in depth-dose calculations within individual mesh cells, up to a depth of 10 cm, were less than 0.4% at one standard deviation (SD). The relative statistical uncertainties of dose along the central axis at depths from 10 cm to 30 cm were $< 0.6\%$. Additionally, the MC-based statistical uncertainties of $< 0.6\%$,

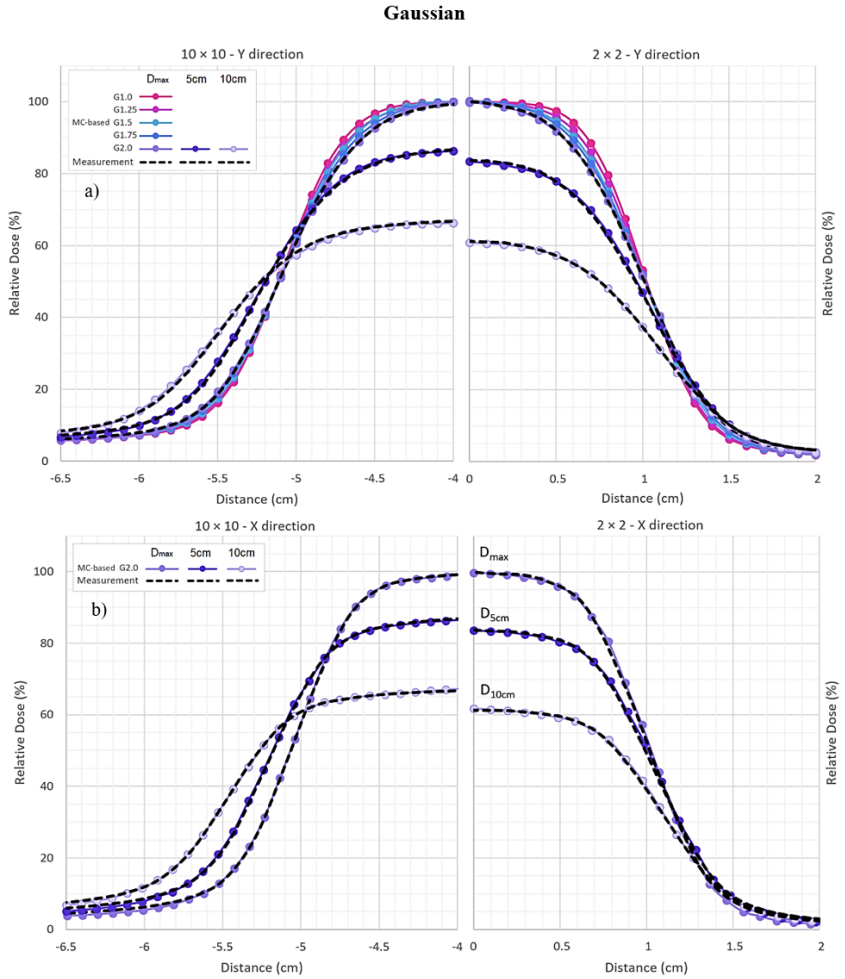

Figure 3: The lateral beam profiles in (a) y-, and (b) x-directions for 10×10 cm^2, and 2×2 cm^2 beams considering the gaussian spatial sampling for primary electron beam. The source FWHM = 2 mm was used in all plots, except inline profiles (y-direction) at Dmax, where profiles for all assumed source FWHM of 1.0, 1.25, 1.5, 1.75, and 2.0 mm were shown.

$< 1.2\%$, and $< 2.4\%$ were obtained for dose profiles in the in-field, penumbra, and out-of-field regions, respectively. However, there were still some random fluctuations in the experimental PDD and LDP raw data. To address this, the data were processed using PTWs MEPHYSTO® Navigator software. All scanned PDDs and LDPs were smoothed using a similar algorithm with equidistant data points (i.e., two or fewer passes of smoothing) (Das et al., 2008).

The Monte Carlo (MC) model was benchmarked against experimental measurements according to the methodology described by Almberg et al. (Almberg et al., 2012). PDDs for a 10×10 cm^2 field were employed to determine the mean energy of the incident electron beam. In contrast, LDPs for various field sizes were used to determine the spatial distribution of the primary electron source.

Percent Depth Dose (PDD): Figure 2 presents the PDDs for a 6 MV flattened 10×10 cm^2 beam at different mean energies of the primary electrons. In Fig. 2, the dose differences between MC-based and measured data are also displayed. Considering an acceptable dose difference (DD) threshold of $\pm 0.5\%$, mean electron energies of 6.4, 6.5, and 6.6 MeV showed strong agreement with the measured data beyond the build-up region (i.e., depth ≥ 1.5 cm). However, the 6.6 MeV electron beam showed better agreement with measurements than the 6.4 and 6.5 MeV beams in the build-up region. Although higher electron energies (6.8 and 6.9 MeV) showed smaller DDs in the build-up region, they were not selected because of larger deviations from the measured data at greater depths. Based on these findings, the mean electron energy of 6.6 MeV was determined to be the optimal mean energy of the primary electron beam.

Lateral Depth Dose (LDP): To validate the LDPs, MC-based relative doses in both x- and y-directions (i.e., crossline and inline) were compared with the corresponding experimental measurements for all field sizes. Figure 3 shows LDPs for two fields of 2×2 cm^2 and 10×10 cm^2 along the y- and x- directions, respectively. As shown in Fig. 3, LDPs for a source with 2.0 mm FWHM are in good agreement with the measured data for both the small (i.e., 2×2 cm^2) and standard field sizes (i.e., 10×10 cm^2). For both the uniform and Gaussian distributions, excellent agreement was achieved within the in-field region. Beam profiles for the uniformly distributed source

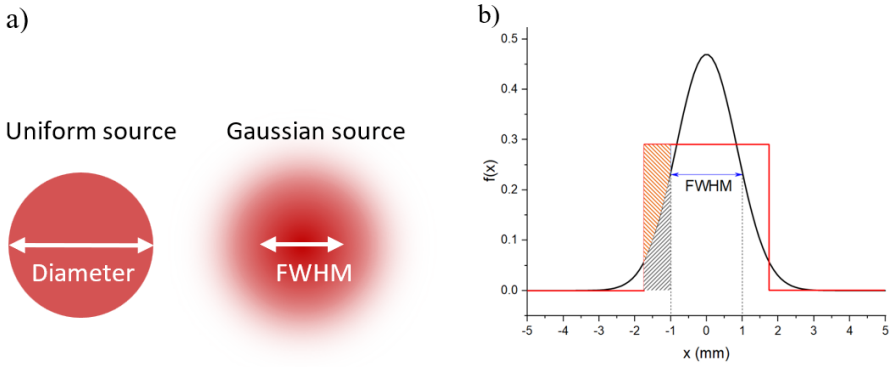

Figure 4: Comparison between uniform and Gaussian source spatial sampling; a) a schematic 2D illustration and b) frequency of source points with respect to lateral direction.

with a 3.5 mm diameter were found to be consistent with those obtained using a Gaussian distribution with a 2.0 mm FWHM. The only notable difference between the two source distributions occurred in the out-of-field region and at depths of 5 cm and 10 cm for larger field sizes, where the uniformly distributed source (3.5 mm diameter) produced doses up to 1.5% higher than the measured data (see Fig. 4). Figure 3 shows that good agreement (i.e., differences of $\leq 0.6\%$) was achieved for beam profiles in the out-field region when assuming a Gaussian distributed source with a FWHM of 2.0 mm.

Output Factors: Figure 5 presents the output factors as a function of field size for both CC04 ion chamber measurements and MC simulations. The output factors were normalized to a 10×10 cm^2 reference field at a depth of 10 cm. The statistical uncertainties for MC-based output factors are $< 1.0\%$ for all field sizes. This figure shows a good agreement between MC-based and measured data. The most significant discrepancy, observed in the 20×20 cm^2 field, was less than 0.63%, within the simulation's relative uncertainty.

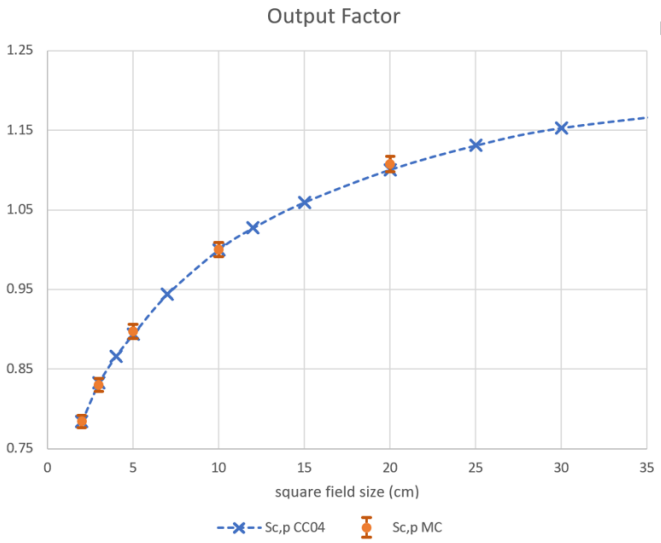

Figure 5: Output factors (Sc,p) for Artiste 6 MV beam. The cross represents CC04 measurements, and circle represents MC data. The output factors are normalized to a 10×10 cm^2 reference field at depth of 10 cm.

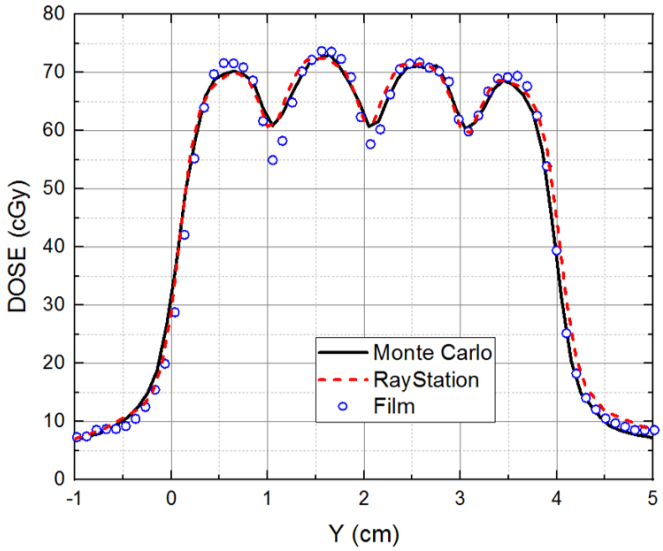

Figure 6: The MC-based dose map for FOURL test field and the comparison of MC-based, RayStation and film measurement profiles.

3.2 MLC test

The MC-based, TPS-based, and measured dose profiles across the leaf-side junctions (at the lower right part of the field) are illustrated in Fig. 6. All three profiles demonstrate a reduction in the delivered dose at the leaf-side junctions. Notably, the comparison of dose profiles shows good agreement between MC-based and TPS-based data (DDs $< 3\%$). Both computational approaches effectively predict the measured dose distributions, except for one valley associated with interleaf leakage. The dose differences (DD) values for these valleys are approximately 10%, 5%, and $< 0.5\%$ for left to right, respectively. We expect the dose reduction to be the same for all three leaf-side junctions, as illustrated by both computational profiles. Therefore, it might be a measurement problem in the film dosimetry process.

3.3 IMRT treatment plan simulation

Monte Carlo simulations for a typical nasopharyngeal IMRT plan with nine gantry angles and 10 to 25 segments

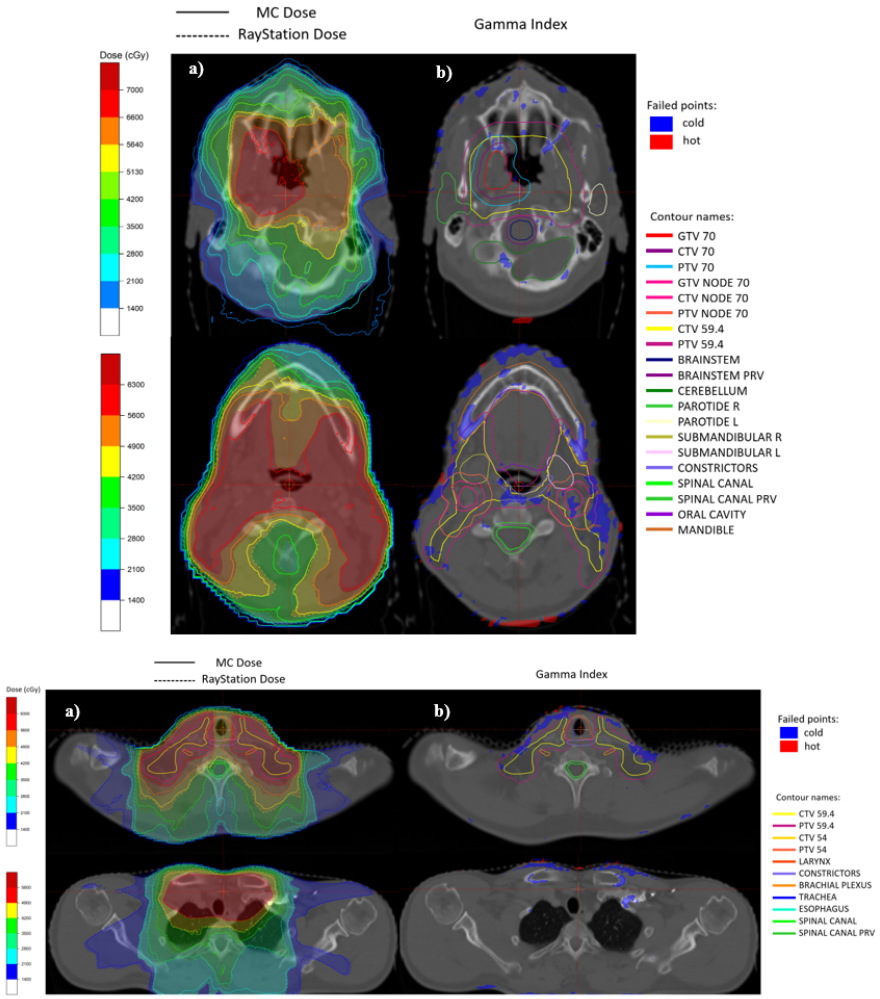

Figure 7: a) MC-based and TPS-based (i.e., RayStation) isodose maps and b) map of gamma failed points. Note: the gamma-passed points are set to be transparent.

per beam were performed until the statistical uncertainty for individual voxels within the field region was $< 2.5\%$. For the beam at a gantry angle of 80°, the MC-based and TPS-based isodose maps are shown in the first column of Fig. 7. As shown, the differences between the two dose calculation methods are in excellent agreement across both target regions and OARs. In the second column of Fig. 7, maps of failed points for comparing the MC-based and RayStation convolution dose distributions (with a 3%/3 mm criterion) were displayed. The 2D GPRs that meet the 3%/3 mm and 10% dose threshold requirements are 97.0%, 98.9%, 99.4%, and 98.7% for the selected slices, respectively. Meanwhile, the 2D GPRs with criteria 3%/2 mm are 96.0%, 98.0%, 99.0%, and 97.7% for the same slices, respectively. The 3D GPRs with criteria 3%/3mm and a dose threshold of 10% are 97.1%, respectively. In Fig. 8, DVH histograms of MC-based and TPS-based calculations related to GTV70, GTV NODE 70, CTV 59.4, CTV 54, brain stem, and temporal lobes of a nasopharyngeal patient are shown. The graphs indicate a significant correlation between the Monte Carlo and RayStation calculations within the target areas. A satisfactory agreement has also been achieved for the identified healthy organs.

4 Discussion

The dose profiles show a negligible energy dependence in the energy range of 6 MeV to 7 MeV, allowing for visual optimization of the primary electron mean energy striking the X-ray target by comparing MC-based and measured PDDs (López-Sánchez et al., 2019; Glenn et al., 2020). The optimized mean energy was selected to best align with both the build-up and fall-off regions. According to the dose differences shown in Fig. 2, the higher energies, e.g., 6.8 and 6.9 MeV, are better confined in the build-up region (with DD values $< 1\%$ and an average of 0.3%). In contrast, in the fall-off region intermediate energies of the considered range seem to be preferred (with DDs of $< 0.5\%$ and the average of 0.3, while in the fall-off region intermediate energies of the considered range seem to be preferred (with DDs of $< 0.5\%$ and the average of 0.3%). Consequently, the manufacturer-provided energy of 6.6 MeV was determined to be the most suitable and accurate for MC calculations. For the optimized energy of 6.6 MeV, the most considerable depth-dose differences were observed in the build-up and surface regions at depths less than 1.5 cm. This discrepancy can be attributed to the detector's sensitive volume (0.08 cm^3 with a 4 mm diameter), which

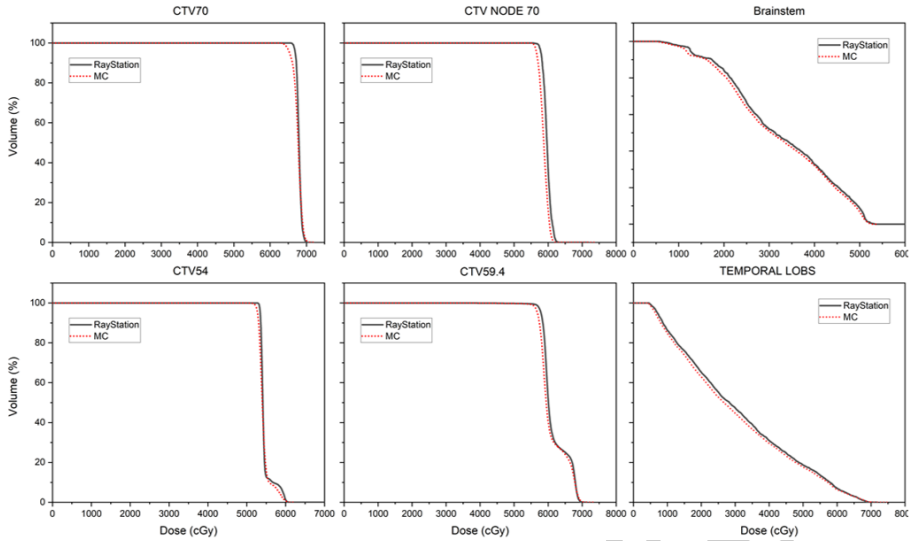

Figure 8: DVH curves comparison between MC and TPS dose data for CTV 70 Gy, CTV NODE 70 Gy, CTV 59.4 Gy, CTV 54 Gy, Brainstem, and temporal lobes.

leads to an over-response in the dose measurement near the surface (Das et al., 2008; Apipunyasopon et al., 2013). Several investigations have carried out approximations to determine the primary electron beam characteristics in Monte Carlo simulation for various linac types (Tuğrul and Eroğul, 2019; Almberg et al., 2012; Sheikh-Bagheri and Rogers, 2002; Tzedakis et al., 2004; Pena et al., 2007; Wang and Leszczynski, 2007). From these studies, the optimal mean electron energy has been estimated by tuning MC-based dose distributions to the measured data.

Determining the primary electron beam size in linear accelerators is a critical factor in ensuring accurate dose delivery in clinical settings. By comparing MC-based and measured LDPs, researchers have effectively assessed the dimensions of the electron beam, as noted in various studies (Almberg et al., 2012). Few authors reported the size of the electron beam for Siemens linacs (Wang and Leszczynski, 2007; Jaffray et al., 1993), particularly the Artiste model. For instance, Turul et al. (Tuğrul and Eroğul, 2019) reported an FWHM of 3.0 mm for a Gaussian-distributed source model, which is roughly consistent with the findings in this study. Other studies have reported different focal spot sizes for specific linac models (Sheikh-Bagheri and Rogers, 2002; Chang et al., 2014; Keall et al., 2003; Sham et al., 2008), indicating that optimization of MC source parameters is essential for each machine used in clinical practice. Some studies considered a uniform source distribution with a fixed diameter (Sham et al., 2008; Hartmann Siantar et al., 2001; Fix et al., 2001). However, Jaffray et al. (Jaffray et al., 1993) demonstrated that electron sources were approximately Gaussian in shape, noting that focal spots are generally circular for both Siemens and Varian machines. The investigation also highlighted that the optimized size of the primary electron source is influenced by the spatial distribution of the source. Based on the results, LDPs from a uniform-source model with a 3.5 mm diameter closely match those from a Gaussian-source model with a 2.0 mm FWHM, especially within the field region. However, in the out-field region, the uniformly distributed source resulted in a 1.5% dose overestimation for larger fields at depths of 5 and 10 cm. This discrepancy arises from intensity variations at source points outside the FWHM, where the uniformly distributed source generates more particles in regions that contribute to dose overestimation just beyond the field boundaries (see the hatched area in Fig. 4).

Furthermore, according to the recommendations for IMRT verification quality assurance by AAPM TG-218, the GPR should be greater than 95%, with a 3%/2 mm threshold and a 10% threshold (Miften et al., 2018). The results show that the 2D gamma passing rates with clinically acceptable criteria of 3%/3 mm, as well as the tighter TG-218 criteria of 3%/2 mm, exceed 97.0% and 95.0%, respectively, indicating acceptable agreement between the MC-based calculations and those from TPS. However, the analysis identified that most failures occurred in specific areas: the surface region, the edges of certain segments, and interfaces between inhomogeneous regions. As noted by Paschal et al., inaccuracies in surface area calculations can arise from failing to account for elements such as thermoplastic masks and head supports in TPS dose computations (Paschal et al., 2022). Additionally, discrepancies at the edges of specific segments may stem from variances in MLC opening adjustments between MC simulations and TPS modeling. Interestingly, the lowest GPR values were observed in the first slice among those evaluated, primarily because of its more heterogeneous composition. In the presence of heterogeneitiesc -especially in complex fields- it is common to observe discrepancies between dose maps obtained from different calculational or experimental dosimetry methods (Snyder et al., 2019; Narayanasamy et al., 2017).

Several modeling assumptions and limitations of the present framework should be acknowledged. In the present study, the treatment room geometry -including bunker walls, floor, ceiling, and ancillary room components- was

not explicitly simulated during the Monte Carlo phasespace generation. This modeling choice is intentional and consistent with a large body of Monte Carlo-based dosimetric studies focusing on infield dose estimation. Notably, none of these established approaches includes a full simulation of the treatment room environment for clinical photonbeam dose calculation. Two fundamental reasons justify this approach: (1) Negligible Contribution to In-Field Dose: For megavoltage photon beams -particularly at 6 MV, as used in this study- the contribution of scatter from bunker walls and room components to the infield dose region is negligible compared to the dominant contributions from the linac head, beam modifiers, and patientrelated scatter. Including room geometry substantially increases computational complexity and runtime while providing no clinically meaningful improvement in infield dosimetric accuracy. Given that computational time is already a central challenge in full Monte Carlo simulations of complex IMRT plans, adding elements that do not significantly contribute to the dosimetric quantities of interest would be impractical and unjustified. (2) Absence of Clinically Relevant Neutron Production: The study is restricted to 6 MV photon beams. It is well known that for photon energies below 10 MV, secondary neutron production is not clinically relevant. This further supports the decision to avoid unnecessary modeling complexity. Accordingly, the exclusion of treatment room geometry has been explicitly stated as a known limitation, along with a detailed justification based on prior Monte Carlo investigations cited in the literature.

Regarding the treatment couch, we acknowledge that in posterior beam arrangements, the couch may intersect the beam path and affect dose distributions. This issue is now clearly stated as a limitation. However, in the present validation stage, our primary objective was consistency with the clinical TPS used for comparison, which did not include the model couch. For this reason, the couch was intentionally excluded at this stage of the study. As noted in the manuscript, the couch model has been incorporated in subsequent stages of our ongoing work.

The process of generating secondary-phase-space files for each beam took approximately. 10-15 minutes, followed by a dose distribution calculation within the patient's body, which, for all 9 beams, was completed in under 2 hours using an Intel Xeon Gold CPU. In addition, the entire simulation workflow has been fully automated. The developed framework directly reads DICOM RTPlan files, extracts segmentspecific MLC leaf positions, and automatically generates the corresponding MCNPX input files, substantially improving efficiency and facilitating future clinical and research applications.

This efficiency highlights the potential for real-time verification of IMRT treatment plans via MC-based calculations with MCNP. Given that the Monte Carlo method is recognized as the gold standard for dose calculation, its application in a real-time adaptive context is particularly promising. However, the main bottleneck of Monte Carlo calculation methods is the relatively long computation time required for MC-based dose calculations, which exceeds the feasible time limit of several minutes. To overcome this shortcoming, we should use appropriate variance-reduction methods in our calculations to reduce computation time and develop real-time MC-based dose verification software.

5 Conclusions

Our overall aim was to provide an MC-based independent dose verification program that can be used in clinical routines. Acceptable agreement of 2D GPRs of $> 97.0\%$ (with criteria 3%/3 mm) and $> 95.0\%$ (with criteria 3%/2 mm) was obtained for complicated IMRT beams. Furthermore, the feasible computation time for each IMRT beam ($\sim$10-15 minutes) allows the completion of a Monte Carlo simulation for all nine IMRT beams within two hours, advancing toward a real-time MC-based dose verification software.

Conflict of Interest

The authors declare no potential conflict of interest regarding the publication of this work.

Funding

The authors declare that no funds, grants, or other financial support were received during the preparation of this manuscript.

References

Almberg, S. S., Frengen, J., Kylling, A., et al. (2012). Monte Carlo linear accelerator simulation of megavoltage photon beams: independent determination of initial beam parameters. *Medical Physics*, 39(1):40–47.

Apipunyasopon, L., Srisatit, S., and Phaisangittisakul, N. (2013). An investigation of the depth dose in the build-up region, and surface dose for a 6-MV therapeutic photon beam: Monte Carlo simulation and measurements. *Journal of Radiation Research*, 54(2):374–382.

Chang, K.-P., Wang, Z.-W., and Shiau, A.-C. (2014). Determining optimization of the initial parameters in Monte Carlo simulation for linear accelerator radiotherapy. *Radiation Physics and Chemistry*, 95:161–165.

Chetty, I. J., Curran, B., Cygler, J. E., et al. (2007). Report of the AAPM Task Group No. 105: Issues associated with clinical implementation of Monte Carlo-based photon and electron external beam treatment planning. *Medical Physics*, 34(12):4818–4853.

Das, I. J., Cheng, C.-W., Watts, R. J., et al. (2008). Accelerator beam data commissioning equipment and procedures: report of the TG-106 of the Therapy Physics Committee of the AAPM. *Medical Physics*, 35(9):4186–4215.

Fix, M. K., Stampanoni, M., Manser, P., et al. (2001). A multiple source model for 6 MV photon beam dose calculations using Monte Carlo. *Physics in Medicine & Biology*, 46(5):1407–1427.

Girardi, A., Fiandra, C., Giglioli, F. R., et al. (2019). Small field correction factors determination for several active detectors using a Monte Carlo method in the Elekta Axesse linac equipped with circular cones. *Physics in Medicine & Biology*, 64(11):11NT01.

Glenn, M. C., Peterson, C. B., Followill, D. S., et al. (2020). Reference dataset of users' photon beam modeling parameters for the Eclipse, Pinnacle, and RayStation treatment planning systems. *Medical Physics*, 47(1):282–288.

Hartmann Siantar, C., Walling, R., Daly, T., et al. (2001). Description and dosimetric verification of the PEREGRINE Monte Carlo dose calculation system for photon beams incident on a water phantom. *Medical Physics*, 28(7):1322–1337.

Hendricks, J. S., McKinney, G. W., Fensin, M. L., et al. (2008). MCNPX 2.6. 0 Extensions. *Los Alamos National Laboratory*, page 73.

Hernandez, V., Angerud, A., Bogaert, E., et al. (2022). Challenges in modeling the Agility multileaf collimator in treatment planning systems and current needs for improvement. *Medical Physics*, 49(12):7404–7416.

IMPAC (2020). IMPAC Medical Systems Inc. Monaco technical reference – post modeling adjustment of MLC parameters, version 2.00. Sunnyvale, CA: IMPAC Medical Systems. *IMPAC Medical Systems*, page 1.

Jaffray, D., Battista, J., Fenster, A., et al. (1993). X-ray sources of medical linear accelerators: focal and extra-focal radiation. *Medical Physics*, 20(5):1417–1427.

Kandlakunta, P., Momin, S., Sloop, A., et al. (2019). Characterizing a Geant4 Monte Carlo model of a multileaf collimator for a TrueBeam linear accelerator. *Physica Medica*, 59:1–12.

Keall, P. J., Siebers, J. V., Libby, B., et al. (2003). Determining the incident electron fluence for Monte Carlo-based photon treatment planning using a standard measured data set. *Medical Physics*, 30(4):574–582.

Kerns, J. R., Stingo, F., Followill, D. S., et al. (2017). Treatment planning system calculation errors are present in most Imaging and Radiation Oncology Core-Houston phantom failures. *International Journal of Radiation Oncology* Biology* Physics*, 98(5):1197–1203.

Kry, S. F., Glenn, M. C., Peterson, C. B., et al. (2019). Independent recalculation outperforms traditional measurement-based IMRT QA methods in detecting unacceptable plans. *Medical Physics*, 46(8):3700–3708.

Kry, S. F., Molineu, A., Kerns, J. R., et al. (2014). Institutional patient-specific IMRT QA does not predict unacceptable plan delivery. *International Journal of Radiation Oncology* Biology* Physics*, 90(5):1195–1201.

Lewis, R., Ryde, S., Hancock, D., et al. (1999). An MCNP-based model of a linear accelerator X-ray beam. *Physics in Medicine & Biology*, 44(5):1219–1230.

López-Sánchez, M., Pérez-Fernández, M., Fandiño, J. M., et al. (2019). An EGS Monte Carlo model for Varian TrueBEAM treatment units: commissioning and experimental validation of source parameters. *Physica Medica*, 64:81–88.

Miften, M., Olch, A., Mihailidis, D., et al. (2018). Tolerance limits and methodologies for IMRT measurement-based verification QA: recommendations of AAPM Task Group No. 218. *Medical physics*, 45(4):e53–e83.

Narayanasamy, G., Saenz, D. L., Defoor, D., et al. (2017). Dosimetric validation of Monaco treatment planning system on an Elekta Versa HD linear accelerator. *Journal of Applied Clinical Medical Physics*, 18(6):123–129.

Nelms, B. E., Chan, M. F., Jarry, G., et al. (2013). Evaluating IMRT and VMAT dose accuracy: practical examples of failure to detect systematic errors when applying a commonly used metric and action levels. *Medical Physics*, 40(11):111722.

Palmans, H., Andreo, P., Huq, M. S., et al. (2018). Dosimetry of small static fields used in external photon beam radiotherapy: summary of TRS-483, the IAEA–AAPM international Code of Practice for reference and relative dose determination. *Medical Physics*, 45(11):e1123–e1145.

Park, H., Paganetti, H., Schuemann, J., et al. (2021). Monte Carlo methods for device simulations in radiation therapy. *Physics in Medicine & Biology*, 66(18):18TR01.

Paschal, H. M., Kabat, C. N., Papaconstadopoulos, P., et al. (2022). Monte Carlo modeling of the Elekta Versa HD and patient dose calculation with EGSnrc/BEAMnrc. *Journal of Applied Clinical Medical Physics*, 23(9):e13715.

Pena, J., González-Castaño, D. M., Gómez, F., et al. (2007). Automatic determination of primary electron beam parameters in Monte Carlo simulation. *Medical Physics*, 34(3):1076–1084.

Sadrollahi, A., Nuesken, F., Licht, N., et al. (2019). Monte-Carlo simulation of the Siemens Artiste linear accelerator flat 6 MV and flattening-filter-free 7 MV beam line. *PLoS One*, 14(1):e0210069.

Sempau, J., Badal, A., and Brualla, L. (2011). A PENELOPE-based system for the automated Monte Carlo simulation of clinacs and voxelized geometriesapplication to far-from-axis fields. *Medical Physics*, 38(11):5887–5895.

Sham, E., Seuntjens, J., Devic, S., et al. (2008). Influence of focal spot on characteristics of very small diameter radiosurgical beams. *Medical Physics*, 35(7Part1):3317–3330.

Sheikh-Bagheri, D. and Rogers, D. (2002). Monte Carlo calculation of nine megavoltage photon beam spectra using the BEAM code. *Medical Physics*, 29(3):391–402.

Snyder, J. E., Hyer, D. E., Flynn, R. T., et al. (2019). The commissioning and validation of Monaco treatment planning system on an Elekta Versa HD linear accelerator. *Journal of Applied Clinical Medical Physics*, 20(1):184–193.

Stapleton, S., Zavgorodni, S., Popescu, I., et al. (2005). Implementation of random set-up errors in Monte Carlo calculated dynamic IMRT treatment plans. *Physics in Medicine & Biology*, 50(3):429–439.

Tuğrul, T. and Eroğul, O. (2019). Determination of initial electron parameters by means of Monte Carlo simulations for the Siemens Artiste Linac 6MV photon beam. *Reports of Practical Oncology and Radiotherapy*, 24(4):331–337.

Tzedakis, A., Damilakis, J. E., Mazonakis, M., et al. (2004). Influence of initial electron beam parameters on Monte Carlo calculated absorbed dose distributions for radiotherapy photon beams. *Medical Physics*, 31(4):907–913.

Valentin, J. (2002). Basic anatomical and physiological data for use in radiological protection: reference values: ICRP Publication 89: Approved by the Commission in September 2001. *Annals of the ICRP*, 32(3-4):1–277.

Wang, L. L. and Leszczynski, K. (2007). Estimation of the focal spot size and shape for a medical linear accelerator by Monte Carlo simulation. *Medical Physics*, 34(2):485–488.

Zhang, B., Mo, Z., Du, W., et al. (2015). Intensity-modulated radiation therapy versus 2D-RT or 3D-CRT for the treatment of nasopharyngeal carcinoma: a systematic review and meta-analysis. *Oral Oncology*, 51(11):1041–1046.

Zhu, T. C., Stathakis, S., Clark, J. R., et al. (2021). Report of AAPM Task Group 219 on independent calculation-based dose/MU verification for IMRT. *Medical physics*, 48(10):e808–e829.

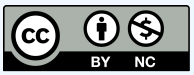

To cite this article:

E. Hoseinian-Azghadi, L. Rafat-Motavalli, H. Miri-Hakimabad, V. Khodabandeh-Baygi, T. Tuğrul, M. Dayyani. Toward a Monte Carlo-driven 3D dose verification framework for IMRT: A pilot implementation for nasopharyngeal carcinoma. *Radiation Physics and Engineering*, In Press.

DOI:

To link to this article: